Active Catheters for Neuroradiology

Jerome Szewczyk[a], Emilie Marchandise[b], Patrice Flaud[c], Laurent Royon[c] and Raphael Blanc[d]

[a] Inst. des Systèmes Intelligents et de Robotique, Université Pierre et Marie Curie (Paris VI), France
[b] Université Catholique de Louvain, Inst. of Materials, Mechanics and Civil Engineering, Belgium
[c] Laboratoire Matière et Systèmes Complexes CNRS, Université Paris Diderot, France
[d] Service de Radiologie, Fondation Rothschild, Paris, France.

Manuscript submitted as :

Regular Paper

Corresponding author :

Jérôme Szewczyk

Institut des Systèmes Intelligents et de Robotique,
Université Pierre et Marie Curie (Paris VI)

Pyramide - T55/65
CC 173 - 4 Place Jussieu
75005 Paris - France

e-mail : jerome.szewczyk@isir.fr
tel. : +33 (0)1 44 27 62 41
fax : +33 (0)1 44 27 51 45

Active Catheters for Neuroradiology

Jerome Szewczyk[a], Emilie Marchandise[b], Patrice Flaud[c], Laurent Royon[c] and Raphael Blanc[d]

[a] Inst. Systèmes Intelligents et Robotique, Université Pierre et Marie Curie (Paris VI), France
[b] Univ. Catholique de Louvain, Inst. of Materials, Mechanics and Civil Engineering, Belgium
[c] Laboratoire Matière et Systèmes Complexes CNRS, Université Paris Diderot, France
[d] Service de Radiologie, Fondation Rothschild, Paris, France.

jerome.szewczyk@isir.fr

List of Figures

List of Tables

Active Catheters for Neuroradiology

Jerome Szewczyk[a], Emilie Marchandise[b], Patrice Flaud[c], Laurent Royon[c] and Raphael Blanc[d]

[a] Inst. Systèmes Intelligents et Robotique, Université Pierre et Marie Curie (Paris VI), France
[b] Univ. Catholique de Louvain, Inst. of Materials, Mechanics and Civil Engineering, Belgium
[c] Laboratoire Matière et Systèmes Complexes CNRS, Université Paris Diderot, France
[d] Service de Radiologie, Fondation Rothschild, Paris, France.

jerome.szewczyk@isir.fr

Abstract

Surgeons performing endovascular interventions have high expectations with regard to the improvement of their operating tools and, more specifically, of their catheters. Active catheters, in which the tip moves actively using shape memory alloy (SMA) actuators, constitute a promising approach. In this article, we review existing SMA-based active catheters present in the literature. We analyze their performances regarding the requirements imparted to neuroradiology. Then, we propose a new analytical model for predicting the thermo-mechanical behavior of steerable catheters actuated through SMA wires. Particularly, we give an expression for the maximal achievable bending angle of the catheter tip. These results are finally applied to the design of single-use small-diameter active catheters especially devoted to neuroradiology. In particular, we present a 3.3-Fr catheter suited for navigating into the Willis' polygon and for accurate positioning into aneurysmal cavities.

Keywords : active catheter, SMA actuator, neuroradiology.

Active Catheters for Neuroradiology

Jerome Szewczyk[a], Emilie Marchandise[b], Patrice Flaud[c], Laurent Royon[c] and Raphael Blanc[d]

[a] Inst. Systèmes Intelligents et Robotique, Université Pierre et Marie Curie (Paris VI), France
[b] Univ. Catholique de Louvain, Inst. of Materials, Mechanics and Civil Engineering, Belgium
[c] Laboratoire Matière et Systèmes Complexes CNRS, Université Paris Diderot, France
[d] Service de Radiologie, Fondation Rothschild, Paris, France.

jerome.szewczyk@isir.fr

1 Introduction

Surgeons performing endovascular surgery (interventional cardiology or neuroradiology, etc...) have high expectations with regard to the improvement of their operating tools and, more specifically, of their catheters. Because of their length and great flexibility, these devices appear to be significantly limited with respect to commandability, precision, and stability. In neuroradiology, in particular, the route through which the catheter must travel from the insertion point (commonly the femoral artery at the groin) to the pathology area (e.g., a cerebral aneurysm) often involves very small vessels with tight radii and large branching angles. Furthermore, neuroradiologists still encounter difficulties in accurately positioning the catheter at the center of the aneurysmal cavity for coil insertion (see Fig. 1).

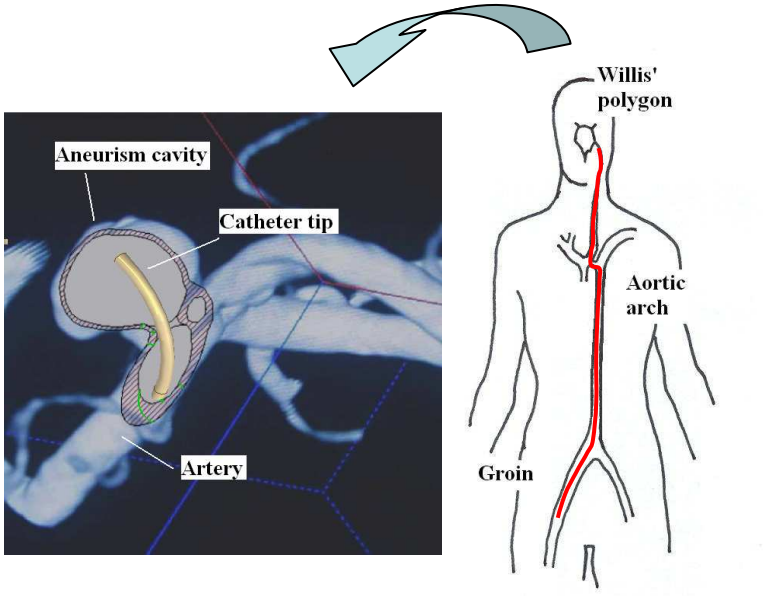

Figure 1: Route of the catheter in the arterial frame.

Various solutions having the form of drivable active catheters were proposed in the literature. For example, Guo et al. [1] imagined a micro-actuator based on the Ionic Conductive Polymer Film (ICPF) technology for controlling the bending of a catheter tip. In Ref. [2], the electrochemical actuation of a catheter coated with polypyrrol is studied. Ikuta et al. [3] produced a hydrodynamic active catheter driven by integrated micro valves. Shape memory alloy (SMA) actuators were also widely investigated. SMA actuators present a number of advantages when applied to active catheterism. They are biocompatible and have an excellent density-to-power ratio [4], [5]. The concept of SMA actuation for catheterism is depicted in Fig. 2. The bending motion is obtained by an electrical current *i* which generates heat by the Joule effect, which induces a phase transformation of the SMA actuator. More than one SMA actuator are generally integrated at the tip of the catheter in order to fully control its bending in the 3-D space. The cross section of a catheter featured with three SMA actuators disposed at 120° from each other is depicted in Figure 3.

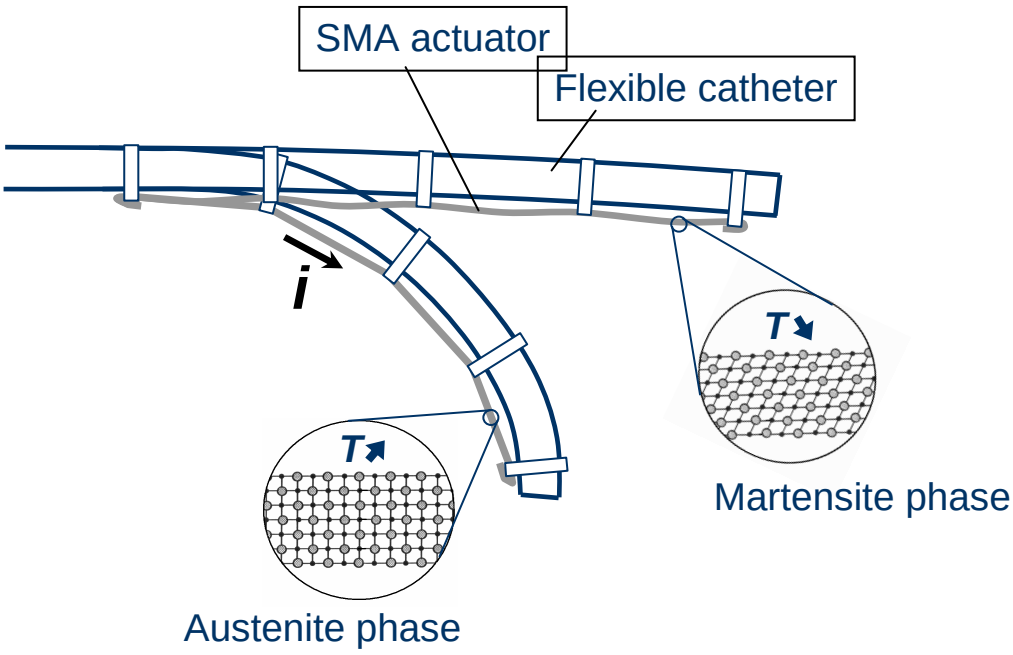

Figure 2: SMA actuated catheter (principle).

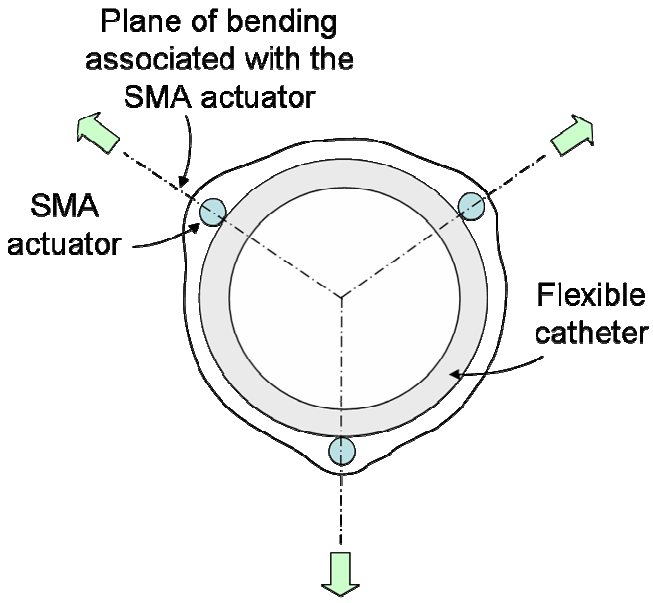

Figure 3: Active catheter featured with three SMA actuators.

Wire-shaped SMA actuators were primarily exploited in the design of active catheters for their simplicity and their high stress capability. For example, Fukuda et al. [6] and Takizawa et al. [7] have developed catheters with external diameters of about 1.5 mm and actuated by three SMA wires distributed at interval of 120° around the catheter. In Ref. [8], a similar device with a diameter of 2.6 mm has been applied to peroral pancreatoscopy in pigs. In Ref. [9], the principle of a catheter having a spiral structure made of a flexible belt integrating SMA wires is presented.

Coil-shaped SMA micro-actuators were also used for their high strain capability [10]. In Ref. [11], the fabrication of a 1.4-mm-diameter catheter using SMA coils as actuators with bending, torsional, and extending control capabilities is detailed. A multi-link active catheter which fabrication is based on silicon micromachining is presented in Ref. [12], together with an interesting method for the indirect heating of the SMA coils. In Ref. [13], a multi-link active catheter including a polyimide-based integrated CMOS interface circuit for communication and control is presented.

SMA actuators having the shape of flat springs have also been used regarding the possibility to produce very small actuators [14]. In Ref. [15], a 0.9-mm-diameter catheter has been

realized this way. More recently, Kubo et al. [16] and Langelaar and Van Keulen [17] studied the feasibility of active catheters cut from thin SMA tubes.

Table 1 summarizes the main characteristics of active catheters with small diameters that have been presented and evaluated in the literature.

Table 1: Performances of active catheters found in the literature.

Authors	Ref	External diameter (mm)	Shape	Number of actuators	Bending angle per unit (deg)	Length of the unit (mm)	Radius of curvature (mm)
Fukuda	[6]	1.65	Wire	3	32	15	27
Mizuno	[8]	2.6	Wire	2	90	20	12.7
Takizawa	[7]	1.5	Wire	3	>45	20	25.5
Mineta	[15]	0.9	Flat spring	3	14	3.1	12.7
Chang	[14]	3.0	Flat spring	3	90	40	25.5
Fu	[10]	1.3	Coil	3	90	92	59
Haga	[11]	1.6	Coil	3	45	19	24.2
Lim	[12]	2.8	Coil	3	13	3	55
Park	[13]	2.0	Coil	3	50	5	5.7

To our knowledge, none of these devices entirely satisfy the constraints imposed by neuroradiology. Applying the concept of active catheterism to neuroradiology indeed raises particular requirements:

(1) Technological complexity and high cost of realization are prohibited with respect to the principle of single-use device.

(2) Diameters close to the millimeter are mandatory because of the thickness of brain arteries.

(3) Most of the time, placing the catheter tip at the center of aneurysm cavities requires radii of curvature to be smaller than 10 mm [18].

As we can see in Table 1, the prototype of Mineta [15] is the only one that simultaneously satisfies the two constraints relative to the diameter and to the radius of curvature. This

prototype is shown in Figure 4. It integrates batch-fabricated small flat NiTi springs as actuators and a three-dimensional super-elastic helicoidal coil as bias spring obtained by photolithography and electrochemical etching. This realization process is complex and poorly compatible with the low-cost constraint.

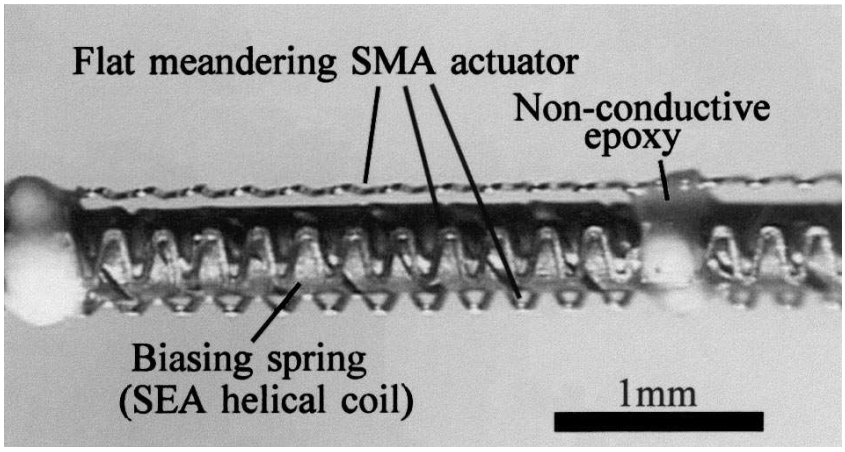

Figure 4: The active catheter of Mineta [15].

In this article, we present a new approach for the design of simple, low-cost, and very small active catheters suited for neuroradiology. Our method is based on a deep understanding of the theoretical behavior of active catheters and the experimental validation of several prototypes. The structure of the article is divided into three parts: (i) First, we present and validate a new kinemato-static behavior model for active catheters featured with SMA wire actuators. (ii) Simple conceptual rules useful for the optimal design of active catheters are derived from this model and two active catheters having the required characteristics for neuroradiological applications are realized. (iii) The performances of these two prototypes are qualitatively evidenced through in-vitro experiments emulating navigation in arteries and embolization of small cerebral aneurysms.

2 Mechanical behavior of SMA-based active catheters

The following kinemato-static model of an active catheter aims to establish the mathematical relations existing between its physical parameters and its main mechanical performances. For

clarity purposes, we will focus on the maximal bending angle the catheter can achieve. Table 2 summarizes our notations.

Table 2: Notations.

σ	radial stress applied by a SMA wire	$\lambda_{\max}$	length of the bendable portion of catheter
T	axial force applied by a SMA wire	$\theta(\lambda)$	bending angle along the neutral axis
r	distance from SMA to the neutral axis	$\theta_{\max}$	total bending angle of the catheter
d	diameter of the SMA wire	$\tilde{\theta}_{\max}$	measured value of the total bending angle
E_A	SMA Young modulus in austenite state	$\tau_{\min}$	strain rate starting the martensite plateau
E_M	SMA Young modulus in martensite state	$\tau_{\max}$	strain rate ending the martensite plateau
E_C	Young modulus of the catheter structure	τ_{init}	rate of pre-strain
λ	local coordinate along the neutral axis	$\hat{\tau}_{init}$	optimal rate of pre-strain

In Ref. [13], the mechanical behavior of an active catheter featured with SMA micro-coils is analyzed relying on the circular bending assumption. In Ref. [10], a more precise model, independent from this assumption, is presented. However, in this model, SMA actuators do not bend with the catheter structure but remain linearly stretched between their fixing points. In Ref. [6], Fukuda et al. address the more realistic case of SMA actuators that always follow the curvature of the catheter. However, the derived expression for the maximal bending angle of the device is not independent from the unknown stress that the SMA wires undergo.

In this section, we give a reliable model for the SMA-based active catheter depicted in Figure 5. It is featured with three wire-shaped SMA actuators having the stress-strain characteristics of Figure 6. In this figure, we also qualitatively indicate the functioning point of each SMA wire in the stress-strain plane when the catheter is at rest and when it is bended.

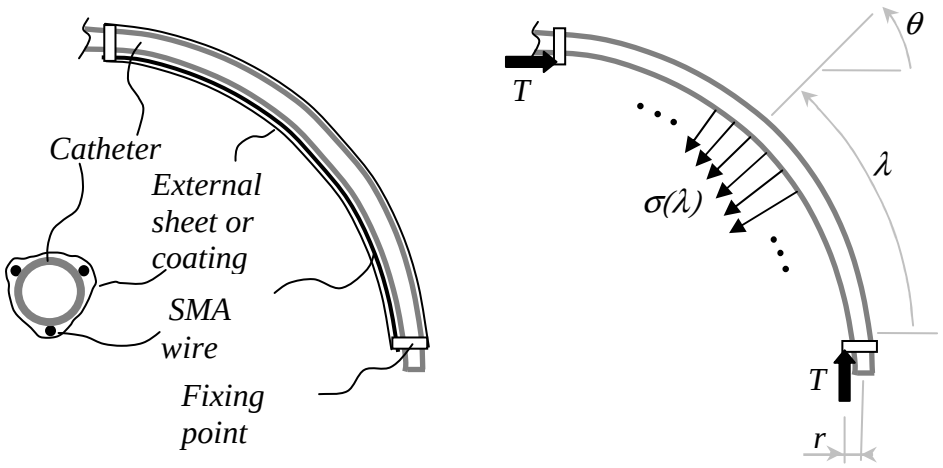

Figure 5: Interaction between an SMA wire and the catheter structure.

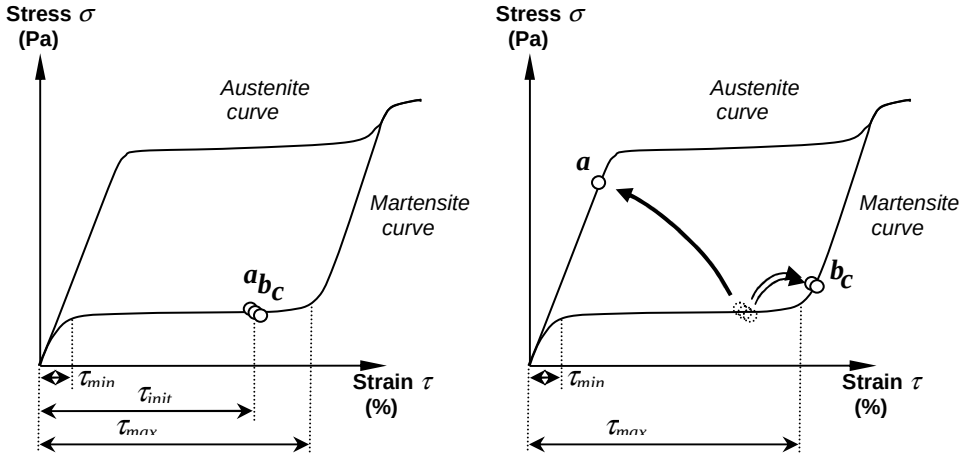

A- Functionning points of the three SMA actuators (*a*,*b*,*c*) when the catheter is straight and at rest

B- Functionning points of the three SMA actuators when the catheter is bended (a : activated wire, b & c : passive wires)

Figure 6: Thermo-mechanical behavior of the SMA actuators.

The mechanical load applied by an SMA wire (either activated or not) to the structure has two components : (1) a compression force *T* applied at the two fixing points, and (2) a shear stress σ distributed along the structure between the two fixing points and located into the bending plane (see Fig. 5).

The shear stress $\sigma(\lambda)$ applied by an SMA wire (either activated or not) to the catheter uniquely depends on the axial force *T* it produces and on the local curvature of the structure:

$$\sigma(\lambda) = T \cdot \frac{\partial \theta(\lambda)}{\partial \lambda} \qquad (1)$$

where λ and θ are respectively the curvilinear coordinate and the bending angle at a specific point of the neutral axis.

In the following, it is assumed that among the three SMA wires, only one is activated and fully austenite transformed while the two others remain in their martensite state and resist to the flexion. Using Relation (1), one can also demonstrate (see Appendix A) that the bending moment applied by an SMA wire is constant along the structure and proportional to the difference between the force T_A applied by the activated wire and the force T_M applied by one passive wire:

$$M = r \cdot (T_A - T_M) \tag{2}$$

Assuming that the catheter material is homogenous, this implies that the curvature $\frac{\partial \theta(\lambda)}{\partial \lambda}$ is constant and that the shape of the bended catheter is circular.

Using Equation (2) in the context of large deflexions, one can derive an expression for the maximal bending angle $\theta_{\max}$ a catheter featured with three SMA wires can reach. The expression of $\theta_{\max}$ depends on the pre-strain τ_{init} identically imposed to the three SMA wires during the assembly process. Assuming that the distance *r* is close to the catheter radius, it can be seen that (see Appendix B):

$$\theta_{\max} \approx \frac{\lambda_{\max}}{r}\left(\tau_{init} - \frac{E_M}{E_A}\tau_{\min}\right)\left(1 + \tau_{init} + \frac{r^2 E_C}{d^2 E_A}\right)^{-1} \text{ if } \tau_{init} \le \hat{\tau}_{init} \tag{3}$$

$$\theta_{\max} \approx \frac{\lambda_{\max}}{r}\left(\tau_{\max} - \frac{E_M}{E_A}\tau_{\min}\right)\left(\frac{3}{2}(1 + \tau_{init}) + \frac{r^2 E_C}{d^2 E_A}\right)^{-1} \text{ if } \tau_{init} > \hat{\tau}_{init} \tag{4}$$

Here, $\hat{\tau}_{init}$ is the largest rate of pre-strain τ_{init} that permits to keep the functioning point of the two stretched passive SMA wires on the martensite plateau during the catheter flexion (i.e. their strain τ remains lower than $\tau_{\max}$ (see Figure 6). One can see (see Appendix C) that

$\hat{\tau}_{init}$ also constitutes an optimal choice for τ_{init} that maximizes the angle $\theta_{\max}$. A close approximation for $\hat{\tau}_{init}$ is:

$$\hat{\tau}_{init} \approx \frac{K+1}{K+1.5}\tau_{\max} \quad \text{with} \quad K = \frac{r^2 E_C}{d^2 E_A} \tag{5}$$

Note that Expressions (3) and (4) have been derived assuming that the activated SMA wire in its complete austenite state undergoes an internal stress that remains under the super-elasticity threshold of the material.

Expressions (2) and (3) were experimentally validated by assessing the bending shape and magnitude of the prototype shown in Fig. 7. Its geometrical and physical parameters are presented in Table 3. In this table, we have also reported the theoretical expected value of $\theta_{\max}$ and its maximal uncertainty deduced from the uncertainties on the model parameters. Note that the prototype is featured with a unique SMA actuator. For this reason, we set the parameter E_M to zero in the above expression of $\theta_{\max}$ (no passive SMA wire).

Table 3: Characteristics of the first prototype.

	r (mm)	D (mm)	E_A (GPa)	E_M (GPa)	E_C (GPa)	$\lambda_{\max}$ (mm)	$\tau_{\min}$	$\tau_{\max}$	τ_{init}	$\theta_{\max}$ (rad)
Nominal values	1.2	0.25	30	0	0.9	158	0.015	0.06	0.046	**3.509**
Uncertainties	0.02	0.005	2	0	0.05	2	0.005	0.005	0.005	**0.756**

We powered this first prototype with an electrical current whose intensity varied from 0 to more than 1.1 A. In Fig. 7, we have reported the successive bending configurations reached by the catheter for five different current intensities. As we can see, all these configurations are very close to perfect circles as predicted by our model. The maximal bending angle for this prototype was found to be $\tilde{\theta}_{\max} = 3.90 \pm 0.20$ rad. On the other hand, Expressions (3) and (5) lead to $\theta_{\max} = 3.51 \pm 0.76$ rad.

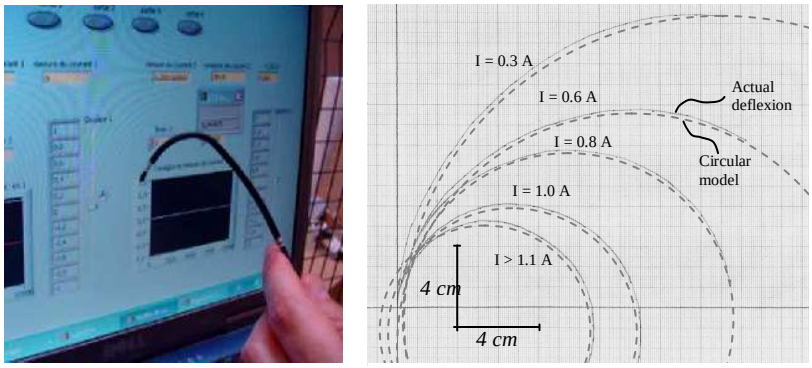

Figure 7: Experimental validation of the model.

3 Two active catheters specially designed for neuroradiology

Regarding Expression (5), it appears that the bending angle $\theta_{\max}$ can be maximized by observing some simple designing rules. Indeed, for a catheter structure with a given size and material, one should:

- Minimize r (i.e. the embedded SMA actuators should lie as close as possible to the neutral axis of the catheter),
- Choose an SMA material that maximizes the parameters $\tau_{\max}$ and E_A,
- Choose the SMA wires' diameter d to be as large as possible, taking into account the limit imposed to the device external diameter.
- Pre-strain the SMA wires with a rate close to $\hat{\tau}_{init}$.

Equation (5) also implies that:

- Applying a scale factor $\alpha < 1$ to r, d and $\lambda_{\max}$ will result in a decrease of the catheter radius of curvature by the same scale factor but will conserve the maximal bending angle $\theta_{\max}$.
- Applying a scale factor $\alpha < 1$ only to r and d will conserve the radius of curvature but will result in an increase of $\theta_{\max}$ by a factor $1/\alpha$..

These recommendations and considerations were applied to the production of two active catheters. The first one is a 2.0-mm external diameter catheter with an internal lumen of 1.4 mm (Fig. 8a).. It emulates a 6-Fr standard guiding catheter useful for navigating from the

insertion point to the carotid artery. As can be seen in Fig. 8(a), its dimensions are compatible with the use of a standard introductor and guide wire. The second one is an ultra-fine catheter having an external diameter of 1.2 mm and an internal lumen of 0.5 mm. It emulates a 3.3-Fr standard micro-catheter suited for the navigation in the tiny brain arteries and the positioning into aneurysmal cavities. The assembly process for both prototypes is very simple as depicted in Fig. 8(b). Insulation can be obtained by covering the distal part of the catheter with a thin sheeth of silicone elastomer like the Silibione™ for example.

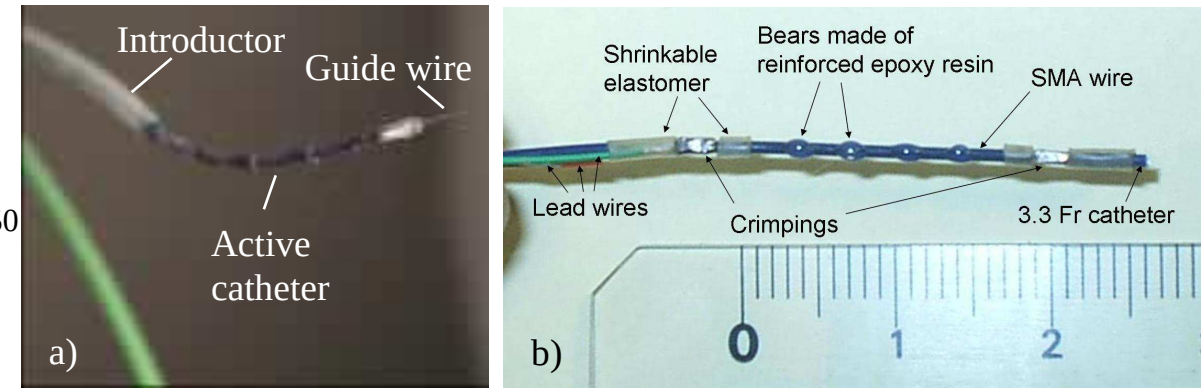

Figure 8: a) Prototype with diameter 6 Fr. b) Details of the realization (before overcoating).

4 Experimental validation of the prototypes

First, the thermal biocompatibility of these devices was verified using the set up shown in Figure 9. Cu-ConstantanT-type thermocouples were used to asses the devices' external surface temperature. For this test, the surrounding water had a controlled temperature of 37°C and a flowing rate of 20 cm/s. Results show that the surface temperature never exceeds 41°C for a constant current intensity up to 2 A. More details on this thermal characterization can be found in Ref. [19].

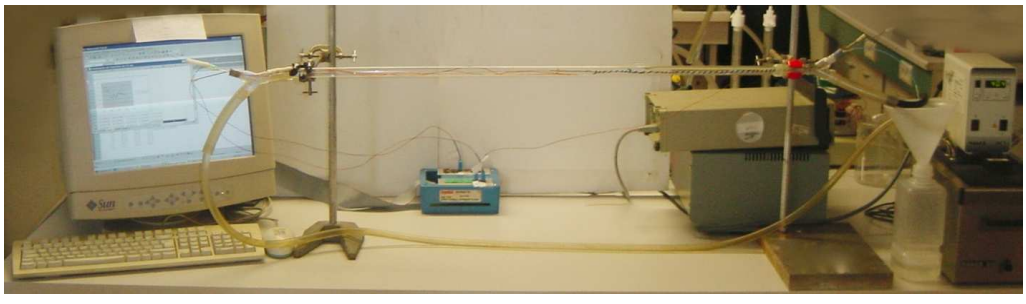

Figure 9: Experimental set-up for temperature assessment.

Then, the performances of the two prototypes were qualitatively evaluated using two realistic 3-D and 2-D anatomical models. Figure 10 shows how the 6-Fr (2mm) prototype allows passage through the aortic arch and entrance to the carotid artery. This task was performed without difficulties by a non-initiated operator.

Figure 10: 6-Fr prototype going through the aortic arch.

Figure 11 shows the 3.3-Fr (1.2mm) prototype progressing into the fine arteries of the Willis' polygon. This experiment shows how SMA actuators can also be used to precisely place the catheter distal extremity at the center of cerebral aneurysms (see pictures 2 and 4 of Fig.11). As depicted in Fig. 11 (picture 4), its maximal bending angle is greater than 70° and its minimal radius of curvature is about 9 mm.

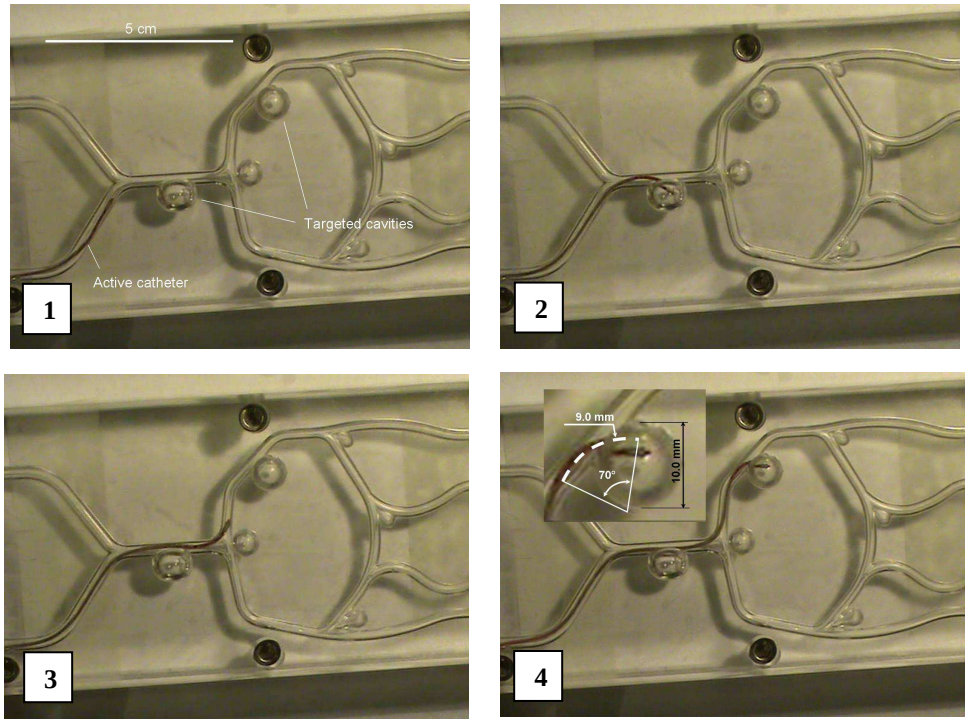

Figure 11: 3.3Fr catheter navigating through the Willis' polygon.

Note also that these two prototypes have sufficient bending rate regarding the targeted medical application. For example, the second prototype can bend to 70° in less than 2 s.

4 Conclusion

Drivable catheters actuated through shape memory alloy are a promising approach for the endovascular treatment of pathologic conditions involving cervical and intracranial vessels. In this article, we have evaluated this concept both analytically and experimentally.

An original kinemato-static model for this kind of device has been presented and tested. It relies on a realistic description of:

1. the mechanical interaction between the SMA wires and the catheter structure
2. the thermo-mechanical behavior of the NiTi material.

Two different prototypes of active catheters were designed based on information derived from the proposed model. They were experimented on realistic anatomical phantoms. Particularly, a 1.2-mm-diameter catheter actuated by SMA wires was realized and proved to be suited for distal extremity controlling and positioning.

In future works, in-vivo evaluations of our prototypes will be conducted in pig and rabbit. Additionally, we will improve our design approach by considering other criteria such as energy consumption and dynamical behavior. For this purpose, a fluid-thermal simulation program describing active catheters evolving in blood is currently under development [19].

5 References

[1] S. Guo et al., Micro Catheter System with Active Guide Wire, IEEE Int. Conf. on Robotics and Automation, pp 79-84, 1995.

[2] T. Shoa et al., Conducting Polymer Based Active Catheter for Minimally Invasive Interventions inside Arteries, IEEE Int. Conf. of the Eng. in Medicine and Biology Society pp 2063-2066, 2008.

[3] K. Ikuta et al., Hydrodynamic Active Catheter with Multi Degrees of Freedom Motion, IFMBE World Congress on Medical Physics and Biomedical Engineering, pp 3091-3094, 2007.

[4] S. Shabalovskaya, On the nature of the biocompatibility and on medical applications of niti shape memory and superelastic alloys, Biomed Mater Eng, Vol. 6 (4), pp 267-289, 1996.

[5] J. Peirs, D. Reynaerts, H. Van Brussel, The true power of SMA micro-actuation, MicroMechanics Europe Workshop, pp. 217-220, 2001.

[6] T. Fukuda, S. Guo, K. Kosuge, F. Arai, M. Negoro, K. Nakabayashi, Micro active catheter system with multi degrees of freedom, IEEE Int. Conf. on Robotics and Automation, pp 2290-2295, 1994.

[7] H. Takizawa, H. Tosaka, R. Ohta, S. Kaneko, Y. Ueda, Development of a Micro fine active bending catheter equipped with mif tactile sensors, IEEE Int. Conf. on Micro Electro Mechanical Systems, pp 412-417, 1998.

[8] S. Mizuno et al., Shape memory alloy catheter system for peroral pancreatoscopy using an ultrathin-caliber endoscope, Endoscopy, Vol. 26(8), pp 676-680, 1994.

[9] Y. Koseki et al., Development of a Spiral Structure for an Active Catheter Overview of the Spiral Structure and Its Kinematic Configuration, IEEE/RSJ Int. Conf. on Intelligent Robots and Systems, Vol. 2, pp. 1259-1264, 1999.

[10] Y. Fu et al., Research on the axis shape of an active catheter, Int. Journal of Medical Robotics and Computer Assisted Surgery, Vol. 4, pp69–76, 2008.

[11] Y. Haga, Y. Tanahashi, M. Esashi, Small diameter active catheter using shape memory alloy, IEEE Int. Conf. on Micro Electro Mechanical Systems, pp. 419-424, 1998.

[12] G. Lim et al., Active catheter with multi-link structure based on silicon micromachining, IEEE Int. Conf. on Micro Electro Mechanical Systems, pp116–121, 1995.

[13] K. Park, M. Esashi, A multilink active catheter with polyamide-based integrated CMOS interface circuit, Journal of Microelectromechanical Systems, Vol. 8 (4), pp 349-356, 1996.

[14] J. Chang, S. Chung, Y. Lee, J. Park, Development of endovascular microtools, Journal of Micromechanics and Micro-engineering, Vol. 12, pp 824-831, 2002.

[15] T. Mineta, T. Mitsui, Y. Watanabe, S. Kobayashi, Y. Haga, M. Esashi, Batch fabricated flat meandering shape memory alloy actuator for active catheter, Sensors and Actuators A, Vol. 88, pp 112-120, 2001.

[16] H. Kubo et al., Fabrication of Microactuator for Active Catheter from SMA Thin Film Tube, 21st Sensor Symposium on Sensors, Micromachines and Applied Systems, pp 39-42, 2004.

[17] M. Langelaar, F. Van Keulen, Design optimization of shape memory alloy active structures using the R-phase transformation, SPIE Conference on Active and Passive Smart Structures and Integrated Systems, pp 6525-6530, 2007.

[18] T. Abe, Distal-Tip Shape-Consistency Testing of Steam-Shaped Microcatheters Suitable for Cerebral Aneurysm Coil Placement, J. of Neuroradiology, Vol. 25, pp 1058–1061, June/July 2004.

[19] E. Marchandise, L. Royon, P. Flaud, and J. Szewczyk, Active catheters prototyping : application for neuroradiology, 5th European Congress on Computational Methods in Applied Sciences and Engineering, 2008.

6 Appendix

Appendix A

We first consider a catheter featured with only one SMA wire. As depicted in Fig. 12, this wire applies to the structure an axial tip force $T = -T\mathbf{x}_0$ and a distributed shear stress $\sigma(\lambda) = -\sigma(\lambda)\mathbf{y}_\lambda$ all along the line it is connected to the catheter. Fig. 13 illustrates the local relation between the stress $\sigma(\lambda)$, the curvature of the catheter $\frac{\partial\theta(\lambda)}{\partial\lambda}$ and the axial force *T*. As we can see, the static equilibrium at any point of the SMA wire implies :

$$\sigma(\lambda) = \frac{2T \cdot \sin(\delta\theta/2)}{\delta\lambda} \approx T \cdot \frac{\partial\theta(\lambda)}{\partial\lambda} \qquad \text{(A-1)}$$

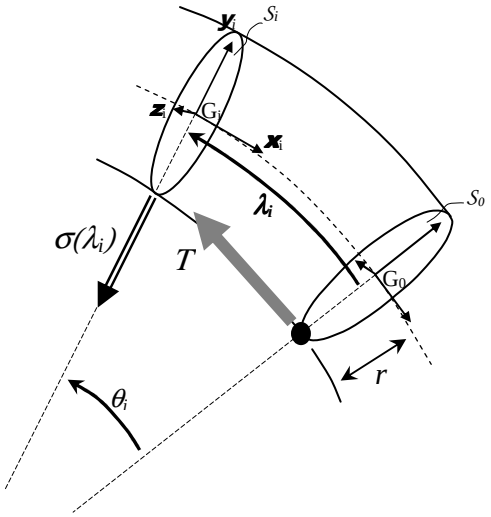

Figure 12: Mechanical interaction between the catheter and the SMA wire.

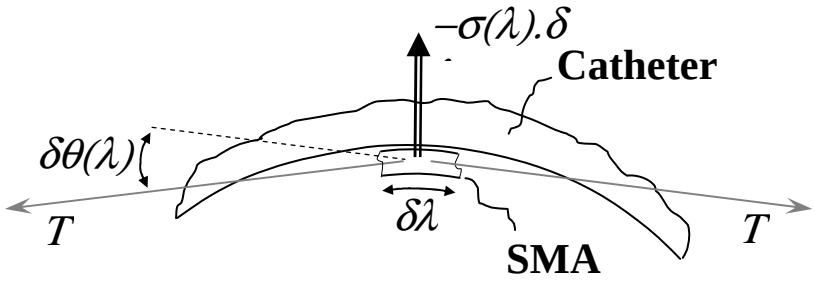

Figure 13: Static equilibrium at any point of the SMA wire.

Let S_1 be a planar transversal section of the bended structure at curvilinear coordinate λ_1. S_1 crosses the neutral axis of the catheter at a point G_1. The static equilibrium of S_1 is described by :

$$\frac{\delta \boldsymbol{M}(\lambda_1)}{\delta\lambda} + \mathbf{x}_1 \times \boldsymbol{N}(\lambda_1) + \boldsymbol{m}(\lambda_1) = 0 \qquad \text{(A-2)}$$

where $\boldsymbol{M}(\lambda_1)$, $\boldsymbol{N}(\lambda_1)$ and $\boldsymbol{m}(\lambda_1)$ are the resulting bending moment, the resulting force and the density of external moment applied to S_1 at G_1, respectively.

Because the stress $\sigma(\lambda)$ is purely radial, $\boldsymbol{m}(\lambda) = 0$ and then:

$$\frac{\delta \boldsymbol{M}(\lambda_1)}{\delta\lambda} = -\mathbf{x}_1 \wedge \boldsymbol{N}(\lambda_1) \qquad \text{(A-3)}$$

The resulting force $\boldsymbol{N}(\lambda_1)$ at G_1 is obtained by summing the actions of the SMA wire on the catheter for λ ranging from 0 to λ_1 :

$$\boldsymbol{N}(\lambda_1) = \boldsymbol{T} + \int_0^{\lambda_1} \boldsymbol{\sigma}(\lambda)\delta\lambda = -T\mathbf{x}_0 - \int_0^{\lambda_1} T \cdot \frac{\partial\theta(\lambda)}{\partial\lambda}\mathbf{y}_\lambda \delta\lambda \qquad \text{(A-4)}$$

By expressing the unit vectors $\mathbf{x}_0$ and $\mathbf{y}_\lambda$ in the base frame attached to the section S_1, relation (A-4) becomes :

$$\boldsymbol{N}(\lambda_1) = T\begin{pmatrix} -\cos(\theta_1) \\ \sin(\theta_1) \\ 0 \end{pmatrix} - \int_0^{\lambda_1} T\left(\frac{\delta\theta(\lambda)}{\delta\lambda}\right)\begin{pmatrix} \sin(\theta_1 - \theta) \\ \cos(\theta_1 - \theta) \\ 0 \end{pmatrix}\delta\lambda$$

$$\boldsymbol{N}(\lambda_1) = T\left[\begin{pmatrix} -\cos(\theta_1) \\ \sin(\theta_1) \\ 0 \end{pmatrix} - \int_0^{\theta_1}\begin{pmatrix} \sin(\theta_1 - \theta) \\ \cos(\theta_1 - \theta) \\ 0 \end{pmatrix}\delta\theta\right]$$

$$\boldsymbol{N}(\lambda_1) = T\begin{pmatrix} -1 \\ 0 \\ 0 \end{pmatrix} = -T\mathbf{x}_1 \qquad \text{(A-5)}$$

Finally, (A-5) into (A-3) yields:

$$\frac{\delta\boldsymbol{M}(\lambda_1)}{\delta\lambda} = 0 \qquad \text{(A-6)}$$

When the catheter is featured with three SMA wires (as the one depicted on Fig. 3), the same result can be obtained accounting for the fact that each SMA wire interacts with the catheter the same way as described in Fig. 12 whatever it is active or passive. In this case, if only one SMA wire is activated while the two others remain passive, the set of axial tip forces applied at the catheter extremity has the configuration shown in Fig. 14. Here, T_M stands for the tip force applied by a passive wire and T_A stands for the tip force applied by the active one. Thus, the resulting bending moment applied to section S_0 is :

$$M = r \cdot (T_A - T_M) \qquad \text{(A-7)}$$

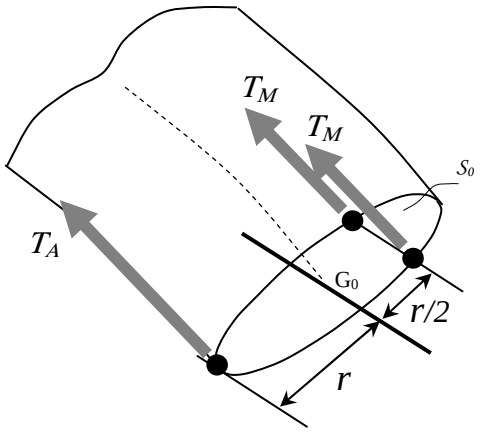

Figure 14: Tip forces applied to the catheter when one SMA is active and two others are passive.

Appendix B

The tip force T_A is related to the axial strain τ_A undergone by the active SMA wire by :

$$T_A = E_A \tau_A \frac{\pi}{4} d^2 \qquad \text{(B-1)}$$

As depicted on Fig. 15, the relation between the tip force T_M and the axial strain τ_M undergone by a passive SMA wire depends on the location of the functioning point of this passive wire on its martensite curve:

$$T_M = E_M \tau_{\min} \frac{\pi}{4} d^2 \qquad \text{if } \tau_M \le \tau_{\max} \text{ (case (i))} \qquad \text{(B-2)}$$

and

$$T_M = E_M \tau_{\min} \frac{\pi}{4} d^2 + E_A (\tau_M - \tau_{\max}) \frac{\pi}{4} d^2 b \qquad \text{if } \tau_M > \tau_{\max} \text{ (case (ii))} \qquad \text{(B-3)}$$

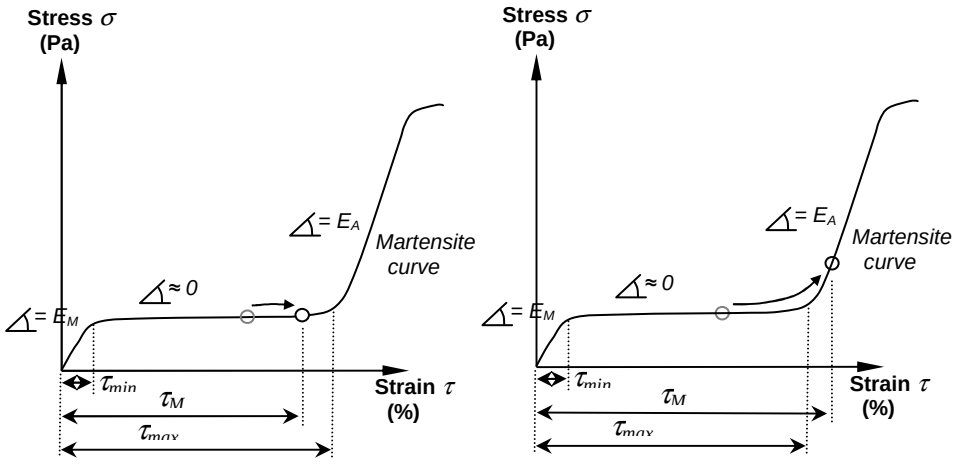

(i) : the functionning point of the two passive wires is such that $\tau_M \le \tau_{max}$

(ii) : the functionning point of the two passive wires is such that $\tau_M \ge \tau_{max}$

Figure 15: Two cases regarding the location of the functioning point of a passive wire on its martensite curve.

Moreover, the strains τ_{init} , τ_A and τ_M are related to the catheter bending angle $\theta_{\max}$ as illustrated in Fig. 16. If L_0 is the original length of the SMA wires (no strain), we have:

$$\theta_{\max} = \frac{L_0(1+\tau_{init})}{R} = \frac{L_0(1+\tau_A)}{R-r} = \frac{L_0(1+\tau_M)}{R+r/2} \qquad \text{(B-3)}$$

and thus :

$$\tau_A = \tau_{init} - \frac{r}{R}(1+\tau_{init}) \quad \text{and} \quad \tau_M = \tau_{init} + \frac{r}{2R}(1+\tau_{init}) \qquad \text{(B-4)}$$

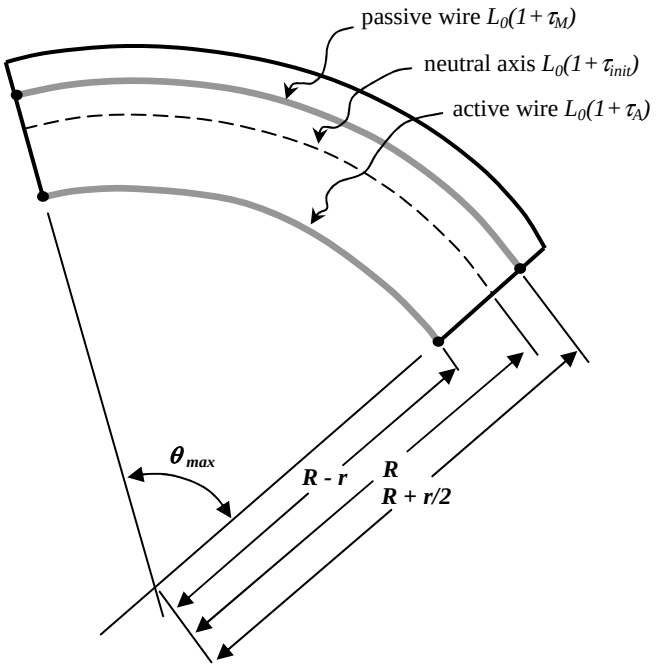

Figure 16: Relations between the strains undergone by the SMA wires when the catheter is bended and their initial pre-strain.

Finally, combining equations (A-7) and (B-1) to (B-4), the constant bending moment applied to the catheter by the three SMA wires can be rewritten as :

$$M = r \cdot \frac{\pi d^2}{4} \cdot \left[E_A(\tau_{init} - \frac{r}{R}(1+\tau_{init})) - E_M \tau_{\min} \right] \quad \text{in case (i)} \qquad \text{(B-5)}$$

and

$$M = r \cdot \frac{\pi d^2}{4} \cdot \left[E_A(\tau_{\max} - \frac{3r}{2R}(1+\tau_{init})) - E_M \tau_{\min} \right] \quad \text{in case (ii)} \qquad \text{(B-6)}$$

Besides, this moment is related to the catheter constant radius of curvature $R = \frac{\lambda_{\max}}{\theta_{\max}}$ by :

$$E_C I_C \frac{\theta_{\max}}{\lambda_{\max}} = M \qquad \text{(B-7)}$$

For thin catheters, a current upper bound of the ratio internal radius / external radius is 0.5. In this case, the quadratic momentum I_C can be approximated by:

$$I_C \approx \frac{\pi r^4}{4} \qquad \text{(B-8)}$$

At least, if we set $Q = \frac{E_M}{E_A}$ and $K = Q\frac{r^2}{d^2}$, combining equations (B-5) to (B-8) gives:

$$\theta_{\max} = \frac{\lambda_{\max}}{r}(\tau_{init} - Q\tau_{\min})(K + 1 + \tau_{init})^{-1} \quad \text{in case (i)} \qquad \text{(B-9)}$$

And

$$\theta_{\max} = \frac{\lambda_{\max}}{r}(\tau_{\max} - Q\tau_{\min})\left(K + 3/2(1+\tau_{init})\right)^{-1} \qquad \text{in case (ii)} \qquad \text{(B-10)}$$

Appendix C

For fixed geometrical and physical parameters, the selection between case (i) and case (ii) only relies on the choice of the pre-strain τ_{init} of the wires. The transition value $\hat{\tau}_{init}$ between these two cases can be derived by equalising expressions (B-9) and (B-10). It leads to :

$$\hat{\tau}_{init}^{\ 2} + b\hat{\tau}_{init} + c = 0 \qquad \text{(C-1)}$$

with

$$b = 1 - \frac{2}{3}(\tau_{\max} + \frac{1}{2}Q\tau_{\min} - K) \quad \text{and} \quad c = -\frac{2}{3}(\tau_{\max} + \frac{1}{2}Q\tau_{\min} + K)$$

This second order equation has a unique solution regarding the positivity of τ_{init} :

$$\hat{\tau}_{init} = \frac{1}{2}(-b + \sqrt{b^2 - 4c}) \qquad \text{(C-2)}$$

which can be closely approximated by :

$$\hat{\tau}_{init} \approx \frac{2K+2}{2K+3}\tau_{\max} \qquad \text{(C-3)}$$

by neglecting some second order terms.

Moreover, the partial derivatives of expressions (B-9) and (B-10) with respect to the pre-strain τ_{init} are :

$$\frac{\delta\theta_{\max}}{\delta\tau_{init}} = \frac{\lambda_{\max}}{r}\frac{K+1+Q\tau_{\min}}{(K+1+\tau_{init})^2} \qquad \text{in case (i)} \qquad \text{(C-4)}$$

and

$$\frac{\delta\theta_{\max}}{\delta\tau_{init}} = \frac{\lambda_{\max}}{r}\frac{-3/2(\tau_{\max} - Q\tau_{\min})}{\left(K + 3/2(1+\tau_{init})\right)^2} \qquad \text{in case (ii)} \qquad \text{(C-5)}$$

The first of these derivatives is always positive while the second one is always negative accounting for the fact that $Q < 1$. Remarking that cases (i) and (ii) correspond to the cases $\tau_{init} \le \hat{\tau}_{init}$ and $\tau_{init} > \hat{\tau}_{init}$ respectively, proves that $\hat{\tau}_{init}$ constitutes an optimal choice for the SMA wires pre-strain τ_{init} which maximizes the catheter bending angle $\theta_{\max}$.